ACS APPLIED MATERIALS & INTERFACES

Research Article

www.acsami.org

Highly Efficient Antibacterial and Pb(II) Removal Effects of Ag-$CoFe_2O_4$-GO Nanocomposite

Shuanglong Ma, Sihui Zhan,* Yanan Jia, and Qixing Zhou*

Key Laboratory of Pollution Processes and Environmental Criteria (Ministry of Education), College of Environmental Science and Engineering, Nankai University, Tianjin 300071, P. R. China

Supporting Information

ABSTRACT: Ag-$CoFe_2O_4$-graphene oxide (Ag-$CoFe_2O_4$-GO) nanocomposite was synthesized by doping silver and $CoFe_2O_4$ nanoparticles on the surface of GO, which was used to purify both bacteria and Pb(II) contaminated water. The Ag-$CoFe_2O_4$-GO nanomaterial was characterized by transmission electron microscopy (TEM), X-ray diffraction (XRD), Fourier transform infrared spectroscopy (FTIR), Raman, X-ray photoelectron spectroscopy (XPS), Brunauer-Emmett-Teller (BET), cyclic voltammetry (CV), and magnetic property tests. It can be found that Ag-$CoFe_2O_4$-GO nanocomposite exhibited excellent antibacterial activity against Gram-negative *Escherichia coli* and Gram-positive *Staphylococcus aureus* compared with $CoFe_2O_4$, Ag-$CoFe_2O_4$, and $CoFe_2O_4$-GO composite. This superior disinfecting effect was possibly attributed to the combination of GO nanosheets and Ag nanoparticles. Several antibacterial factors including temperature, time, and pH were also investigated. It was obvious that *E. coli* was more susceptible than *S. aureus* toward all the four types of nanomaterials. The structural difference of bacterial membranes should be responsible for the resistant discrepancy. We also found that Ag-$CoFe_2O_4$-GO inactivated both bacteria in an irreversibly stronger manner than Ag-$CoFe_2O_4$ and $CoFe_2O_4$-GO. The Pb(II) removal efficiency with all the nanomaterials showed significant dependence on the surface area and zeta potential of the materials. In this work, not only did we demonstrate the simultaneous superior removal efficiency of bacteria and Pb(II) by Ag-$CoFe_2O_4$-GO but also the antibacterial mechanism was discussed to have a better understanding of the interaction between Ag-$CoFe_2O_4$-GO and bacteria. In a word, taking into consideration the easy magnetic separation, bulk availability, and irreversibly high antibacterial activity of Ag-$CoFe_2O_4$-GO, it is the very promising candidate material for advanced antimicrobial or Pb(II) contaminated water treatment.

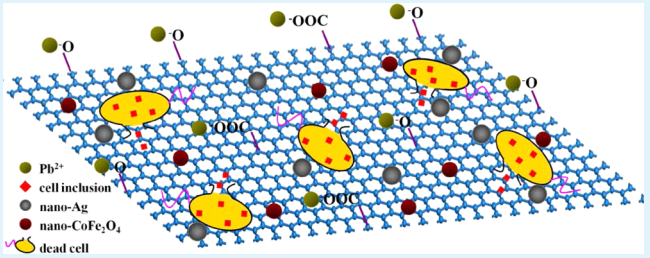

KEYWORDS: *graphene, magnetic separation, nano-Ag, disinfection, Pb(II)*

INTRODUCTION

Microbial contamination has always been the challenge that threats the health of human beings since the existence of human society. Many kinds of bacteria can lead to seriously and even deadly infections for people.[1] Therefore, developing effective, low cost, and environmental biocide is significant and necessary.[2−5] Recently, various antibiotics,[6] silver and gold-based nanomaterials,[7−9] are at the frontline of antibacterial infections. Among these antibacterial substances, antibiotics are popularly used all over the world due to their broad-spectrum antibacterial capacities. However, the antibiotic resistance due to the abuse of antibiotics encourages people to find new alternative antibacterial candidates.[10] Although the silver and gold-based nanomaterials have notable bactericidal activity, the easily oxidized character of silver nanomaterials[11] and the expensive cost of gold limited the application of these two noble metal nanomaterials in practice. Moreover, the silver and gold nanoparticles could not be recycled since they are not separated from the water efficiently, which may result in secondary pollution and serious environmental risk.[12]

On the other hand, Pb(II) pollution is a typical heavy metal contamination which exists in agricultural and industrial wastewater and acidic leachate from landfill sites. Due to their carcinogenicity, high toxicity to the nervous system, and accumulative toxicity,[13−15] the acceptable limit of Pb(II) in drinking water is 0.015 mg/L.[16] The high toxicity and popularity of Pb(II) contamination motivates large amounts of researchers to develop new nanomaterials to resolve the worldwide problem. Many kinds of nanomaterials have been synthesized to remove Pb(II), such as zerovalent iron,[17,18] Fe_3O_4,[19−21] and carbon nanotube-based[22,23] nanomaterials.

Graphene, a two-dimensional single sheet of carbon atoms arranged in a hexagonal network, with exceptional mechanical characteristics,[24] excellent optical transparency,[25] superior electrical conductivity,[26,27] high thermal conductivity,[28] and large surface area,[29] has been intensively studied since it was first discovered by Novoselov and co-workers in 2004.[30]

Received: March 12, 2015
Accepted: April 23, 2015
Published: April 23, 2015

ACS Publications © 2015 American Chemical Society

DOI: 10.1021/acsami.5b02209
ACS Appl. Mater. Interfaces 2015, 7, 10576−10586

Graphene oxide (GO) with a large number of oxygen-containing functional groups such as −COOH and −OH is a highly oxidative form of graphene achieved by chemical exfoliation of graphite.[31] GO also has gained considerable applications in biology and the environmental field due to its bulk availability, high water solubility, and easy modification.[32] The performances of graphene and GO to remove various environmental pollutants have been extensively researched, particularly as absorbers to clear dyes,[33,34] metal ions,[35,36] and organic pollutants[37,38] from contaminated waters. Since fullerenes and carbon nanotubes have been found to have obvious antibacterial properties,[39,40] as the smallest carbon-based nanomaterials, GO and reduced graphene oxide (rGO) have also shown the ability to inhibit the growth of *E. coli* with minimal cytotoxicity.[41,42] Although graphene and GO have rapidly evolved with numerous environmental applications, they could have potential health and ecosystem risks without efficient separation from the environment.[43,44] To overcome this weakness, the synthesis of GO nanocomposites by taking GO as a platform to support magnetic nanoparticles has been studied in the environmental area. The adsorption capacity of graphene-carbon nanotube-iron oxide,[45] Fe_3O_4-rGO,[46] and magnetite-graphene-LDH[47] toward arsenate has been investigated. Graphene-iron oxide-Ag nanocomposite[48] and magnetic-graphene oxide[49] have showed a bactericidal effect.

As we all know, it is necessary for human health to drink safe water free of pollutants such as pathogenic bacteria, organics, and heavy metals. Usually, the ingredients in wastewater are complex including many different kinds of pollutants. Therefore, it is urgent to develop a novel nanomaterial that can be used to remove different pollutants simultaneously. However, to our knowledge, there are few reports about removing multiple pollutants using nanomaterial and especially no report about simultaneous bactericidal and heavy metal ions removal.[50−53] In this study, Ag-$CoFe_2O_4$-GO nanocomposite, combining the high specific surface area of GO, antibacterial capacity of GO and nano-Ag, and magnetic separation property of $CoFe_2O_4$, is synthesized for simultaneous disinfection and Pb(II) removal. The results indicate that Ag-$CoFe_2O_4$-GO nanocomposite shows the highest bactericidal effect with about 98.9% and 74.7% mortality toward *E. coli* and *S. aureus* (10^5 cells/mL), respectively, even at a very low concentration of 6.25 μg/mL compared with $CoFe_2O_4$, Ag-$CoFe_2O_4$, and $CoFe_2O_4$-GO, respectively. In the case of simultaneous disinfection and Pb(II) adsorbing experiments, Ag-$CoFe_2O_4$-GO demonstrates more than 99% of antibacterial efficiency and around 75% of Pb(II) removal efficiency.

EXPERIMENTAL SECTION

Synthesis and Characterization of Ag-$CoFe_2O_4$-GO Nanocomposite. GO nanosheets were synthesized according to the method reported by Hummers and Offeman.[31] Ag-$CoFe_2O_4$-GO nanocomposite was prepared by the solvothermal reaction of $Co(NO_3)_2{\cdot}6H_2O$, $Fe(NO_3)_3{\cdot}9H_2O$, and $AgNO_3$ in the ethanol suspension of GO according to the methods reported by Li et al.[54] and Zhang et al.[55] with some modifications. In brief, 0.12 g of GO was added to 60 mL of ethanol and completely dispersed by ultrasonication for 30 min. 0.1450 g of $Co(NO_3)_2{\cdot}6H_2O$, 0.4025 g of $Fe(NO_3)_3{\cdot}9H_2O$, and 0.1260 g of $AgNO_3$ were dissolved in 20 mL of ethanol and stirred by a magnetic stirrer for 30 min. The solution was added dropwise to the GO suspension and stirred for 30 min. Then, 2.16 g of CH_3COONa was added to the mixture under continuous stirring. After agitation for 30 min, the mixture solution was transferred to a Teflon-line autoclave. The autoclave was heated in an oven at 200 °C for 18 h and cooled down to room temperature. The obtained black composite was washed several times using distilled water and ethanol. Finally, the product was dried in an oven at 60 °C for 18 h. The $CoFe_2O_4$, Ag-$CoFe_2O_4$, and $CoFe_2O_4$-GO were synthesized as discussed in the above method without the addition of $AgNO_3$ and GO, GO, and $AgNO_3$, respectively. The detailed characterization information such as Fourier transform infrared spectroscopy (FTIR), X-ray diffraction (XRD), Raman, and X-ray photoelectron spectroscopy (XPS) was detailed in the Supporting Information.

Bacterial Culture. Gram-negative *E. coli* and Gram-positive *S. aureus* were used as model bacteria. The bacteria were grown in nutrient broth at 37 °C for 24 h to yield a cell count of approximately 10^8 to 10^9 colony forming units (CFU)/mL. Then, bacterial cells were collected by centrifugation (5000*g* for 10 min) and resuspended in sterile 0.85% (wt/vol) saline solution. The bacteria levels for the bactericidal study were 10^5 and 10^3 CFU, respectively, which were adjusted by gradient dilution using phosphate-buffered saline (PBS).

Antibacterial Activity. 50 μL of nanomaterials suspended in PBS were added to 2 mL of bacterial solution, leading to different ultimate concentrations of materials including 6.25, 12.5, 25, and 50 μg/mL. The mixture was incubated by a rotary shaker at 37 °C and 180 rpm for 2 h. Then, the nanomaterials were magnetically separated for 10 min with an external magnet. The supernatant was then carefully pipetted out and determined by the standard plate count method. The plates were incubated at 37 °C for 24 h. The number of colonies was enumerated through visual inspection and that of the bacterial solution without materials was counted as control. A series of experiments were conducted to investigate the antibacterial performance of Ag-$CoFe_2O_4$-GO under different pH values (4, 5, 6, 7, 8, 9), temperatures (298, 303, 310, 315 K), and time intervals (7.5, 15, 30, 60, 120 min). All measurements were carried out in triplicate.

Fluorescent-Based Cell Live/Dead Test. The bacteria death analysis was also ascertained by fluorescent-based cell live/dead test. The mixture of log phase cells (10^8 CFU) and 50 μg/mL nanomaterials was incubated by a rotary shaker at 180 rpm for 2 h. Then, nanomaterials were separated magnetically, and the cells were collected by centrifugation and washed with 0.85% (wt/vol) saline solution three times. Then, the cells were stained with PI (propidium iodide) and SYTO9 (LIVE/DEAD Baclight Bacterial Viability kit) according to the instruction of the kit, then imaged using a laser scanning fluorescence microscope (Olympus, FV1000), and counted by a flow cytometry (CyFlow Space, Partec, Germany). SYTO9 was a cell-permeable green-fluorescent stain that labeled both live and dead bacteria, whereas PI was a cell-impermeable red-fluorescent stain that only labeled cells with compromised cellular membranes. The cell suspension without nanomaterials was taken as control.

Transmission Electron Microscopy and Scanning Electron Microscopy Observation of Bacteria. Transmission electron microscopy (TEM) and scanning electron microscopy (SEM) were used to visualize the interaction between Ag-$CoFe_2O_4$-GO and bacteria. The bacteria treated and untreated with Ag-$CoFe_2O_4$-GO were fixed on a silicon pellet with 2.5% glutaraldehyde solution at 4 °C overnight. Then, the samples were sequentially dehydrated with 30%, 50%, 70%, 90%, and 100% ethanol for 20 min, respectively. The samples were lyophilized, gold sputter-coated, and visualized using a SEM. The pretreatment of TEM samples was similar to SEM except that the TEM samples were fixed on copper mesh.

Simultaneous Disinfection and Pb(II) Adsorption Experiments. $Pb(NO_3)_2$ was used to prepare stock solutions of 100, 200, 400, 600, and 800 mg/L Pb(II), respectively. NaCl solution (0.85%) was used as background electrolyte, for keeping the same background as antibacterial experiments. Before conducting the Pb(II) adsorption experiments, the interaction between bacteria and Pb(II) without nanomaterials was first investigated. The solutions with bacteria (10^5 CFU/mL) and Pb(II) (1, 2, 4, 6, 8 mg/L) were shaken at 37 °C and 180 rpm for 2 h. The individual bacteria and Pb(II) solution at the same concentration was used as a control at the same experimental conditions, respectively. After interaction, the bacteria were counted using the standard CFU counting method, and the Pb(II) was quantitatively measured with the help of an atomic absorption

DOI: 10.1021/acsami.5b02209
ACS Appl. Mater. Interfaces 2015, 7, 10576−10586

spectrometer (IRIS Intrepid II XSP, Thermo Elemental). Batch experiments of Pb(II) adsorption on $CoFe_2O_4$, Ag-$CoFe_2O_4$, $CoFe_2O_4$-GO, and Ag-$CoFe_2O_4$-GO were carried out. In separate experiments, 50 μg/mL of each nanomaterial was added to the Pb(II) solution with different concentrations (1, 2, 4, 6 mg/L). The simultaneous disinfection and the Pb(II) adsorption experiment of each nanomaterial was the same as the individual Pb(II) adsorption method above with the solution containing *E. coli*/*S. aureus* (10^5 CFU/mL).

RESULTS AND DISCUSSION

Characterization of the Antibacterial Nanomaterials. The typical TEM images of the nancomposites are shown in Figure 1. The nano-$CoFe_2O_4$ and silver particles were grown

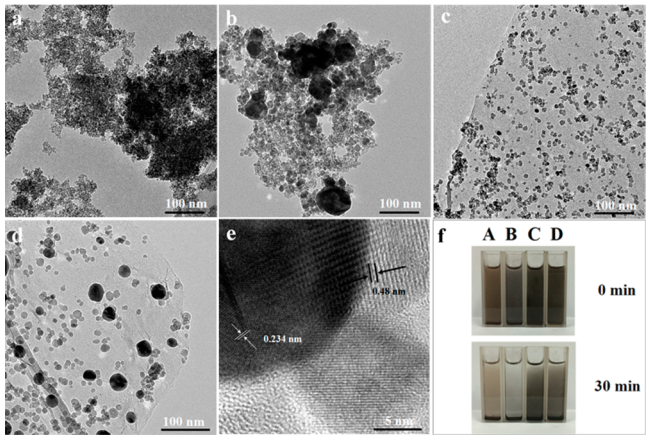

Figure 1. TEM images of $CoFe_2O_4$ (a), Ag-$CoFe_2O_4$ (b), $CoFe_2O_4$-GO (c), and Ag-$CoFe_2O_4$-GO (d) and HRTEM of Ag-$CoFe_2O_4$-GO (e). The dispersity of four nanomaterials is shown in (f). A, B, C, and D represent $CoFe_2O_4$, Ag-$CoFe_2O_4$, $CoFe_2O_4$-GO, and Ag-$CoFe_2O_4$-GO, respectively.

and deposited uniformly on GO nanosheets with narrow particle sizes of 10−20 and 40−50 nm, respectively, as observed in Figure 1c,d. The lattice fringes of $CoFe_2O_4$ (d = 0.48 nm) and Ag (d = 0.234 nm) were shown clearly in Figure 1e. However, $CoFe_2O_4$ and Ag-$CoFe_2O_4$ nanoparticles without GO seriously aggregated, and the Ag nanoparticles in Figure 1b exhibited broad particle size distribution from 50 to 100 nm. Therefore, the presence of GO could stabilize nanoparticles on it and prevent them from aggregation, which was in agreement with the earlier reports.[7,49] Figure 1f showed the dispersities of $CoFe_2O_4$ (A), Ag-$CoFe_2O_4$ (B), $CoFe_2O_4$-GO (C), and Ag-$CoFe_2O_4$-GO (D) in distilled water at 0 and 30 min. It was clear that depositing Ag and $CoFe_2O_4$ nanoparticles on the GO plane could increase the dispersities of Ag nanoparticles and $CoFe_2O_4$. Figure 2a is a representative TEM image of the Ag-$CoFe_2O_4$-GO nanocomposite, with a corresponding energy-dispersive X-ray spectroscopy (EDS) elemental mapping for C (Figure 2b), O (Figure 2c), Ag (Figure 2d), Fe (Figure 2e), and Co (Figure 2f). A brighter area in the elemental map indicated a higher concentration of the corresponding element in that area. Different elements were shown in different colors in order to identify their positions within the nanomaterials. The C distribution was uniform and continuous, resembling the morphology of the GO nanosheet. In contrast, the Ag, Fe, and Co distribution was discrete, indicating a hierarchical heterostructure of nano-Ag and $CoFe_2O_4$ well-dispersed on the GO nanosheet. The scanning transmission electron microscopy

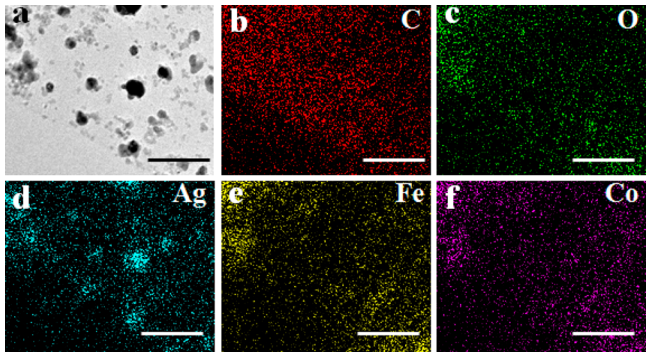

Figure 2. TEM image of Ag-$CoFe_2O_4$-GO nanocomposite (a) and the corresponding energy-dispersive X-ray spectroscopy (EDS) elemental mapping for C (b), O (c), Ag (d), Fe (e), and Co (f). The scale bar is 100 nm.

(STEM)-energy dispersive X-ray (EDX) line scanning was also conducted as shown in Figure S1, Supporting Information, indicating the well distribution of nano-Ag and $CoFe_2O_4$ particles. Other physicochemical characterizations such as FTIR, XRD, Raman spectrum, and XPS exhibited in Figures S2−S7 were discussed in the Supporting Information.

As shown in Figure 3a, the hysteresis loop indicated that the magnetic saturation (Ms) value of the Ag-$CoFe_2O_4$-GO nanoparticles is 0.37 emu/g, whereas the value for $CoFe_2O_4$-GO was 0.13 emu/g as exhibited in the bottom right inset of Figure 3a, suggesting that Ag-$CoFe_2O_4$-GO nanocomposites could be easily separated from solution with an external magnetic force as shown in the top left inset of Figure 3a. All the materials could be easily separated from water with a magnet in 5 min after the antibacterial experiment. The rapid and easy separation of Ag-$CoFe_2O_4$-GO from water after application was significant for not only reusing the absorbent but also avoiding second pollution and serious environmental risk. $CoFe_2O_4$-G and Ag-MnO_2 had been demonstrated as the promising electrode materials for energy storage.[27,56] Therefore, to investigate the electrical conductivity of $CoFe_2O_4$, Ag-$CoFe_2O_4$, $CoFe_2O_4$-GO, and Ag-$CoFe_2O_4$-GO, cyclic voltammograms (CVs) were performed through a three-electrode system with these materials modified glassy carbon electrode as the working electrode, which was prepared by dispersing nanomaterials into anhydrous alcohol, dip coating the uniform dispersion onto the glassy carbon electrode, and drying it in air at room temperature, with a platinum plate as the counter electrode and calomel electrode as the reference electrode. As shown in Figure 3b, all the scans of four nanomaterials in the potential range between 1.0 and −1.0 V in saturated potassium sulfate showed one redox couple. It was obvious that both the oxidative and reduction peaks of Ag-$CoFe_2O_4$-GO were the highest when compared with those of $CoFe_2O_4$, Ag-$CoFe_2O_4$, and $CoFe_2O_4$-GO. It was thus reasonable to relate the high electrical conductivity of Ag-$CoFe_2O_4$-GO to the addition of nano-Ag and graphene into $CoFe_2O_4$.[27,56] The surface areas of $CoFe_2O_4$, Ag-$CoFe_2O_4$, $CoFe_2O_4$-GO, and Ag-$CoFe_2O_4$-GO were 100.4, 89.2, 212.7, and 140.8 m^2/g, respectively (Figure S7, Supporting Information). It was the addition of GO nanosheets that should be responsible for these high surface areas of $CoFe_2O_4$-GO and Ag-$CoFe_2O_4$-GO compared to that of $CoFe_2O_4$ and Ag-$CoFe_2O_4$. Furthermore, materials with high surface areas were in a dominant position in antibacterial and Pb(II) removal performance.

DOI: 10.1021/acsami.5b02209
ACS Appl. Mater. Interfaces 2015, 7, 10576−10586

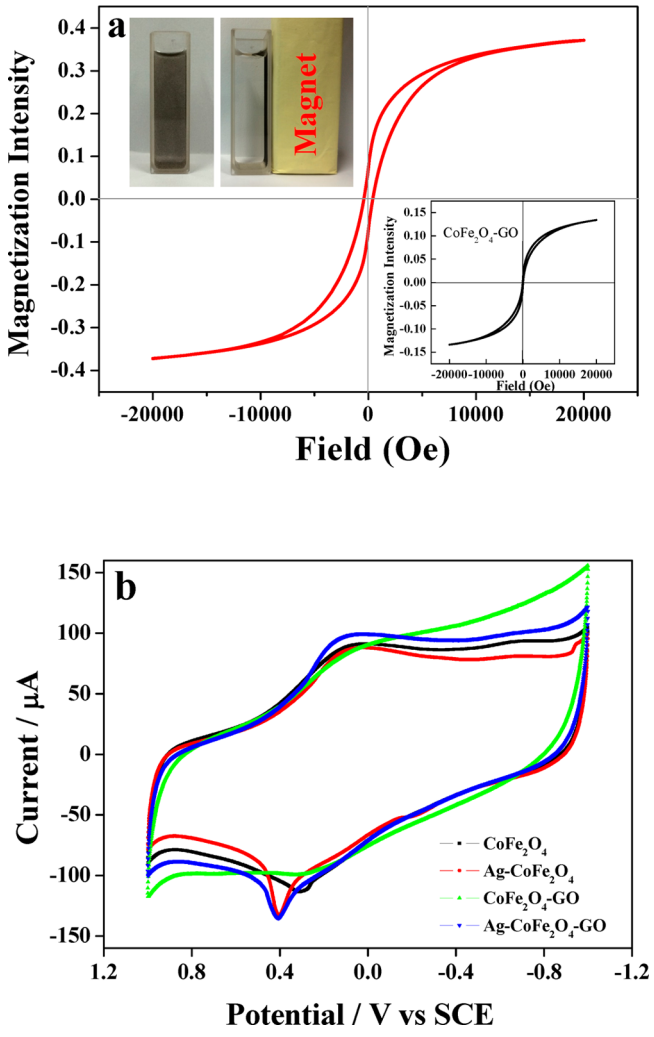

Figure 3. (a) Room temperature magnetization curve of Ag-$CoFe_2O_4$-GO and $CoFe_2O_4$-GO (the bottom right inset); Ag-$CoFe_2O_4$-GO can be easily separated with a magnet (the top left inset). (b) Cyclic voltammetry scans electrodes in 0.1 M sodium sulfate aqueous solution with scan rate of 0.05 V/s.

High Antibacterial Effects of Ag-$CoFe_2O_4$-GO. The antibacterial activities of the four different kinds of nanomaterials ($CoFe_2O_4$, Ag-$CoFe_2O_4$, $CoFe_2O_4$-GO, and Ag-$CoFe_2O_4$-GO) in this work were evaluated using *E. coli* (G−) and *S. aureus* (G+) as model organisms. As shown in Figure 4, all the nanomaterials showed an antibacterial effect toward *E. coli* and *S. aureus* in a dose-dependent manner except for Ag-$CoFe_2O_4$-GO which demonstrated an almost identical antibacterial effect toward *E. coli* as the concentration of material increased (Figure 4A,B). It was obvious that all the nanomaterials showed stronger bacterial inactivation against bacteria with 10^3 CFU/mL than those of 10^5 CFU/mL. Noticeably, Ag-$CoFe_2O_4$-GO in different levels always possessed the best antibacterial effects toward both bacteria. Ag-$CoFe_2O_4$-GO exhibited the highest antibacterial activity with inactivation rates of 98.8% and 73.4% toward *E. coli* and *S. aureus* (10^5 CFU/mL), respectively, even at a concentration as low as 6.25 μg/mL. In this work, the nanocomposites containing nano-Ag exhibit stronger antibacterial effects than $CoFe_2O_4$ and $CoFe_2O_4$-GO. It was well-known that nano-Ag shows an excellent antibacterial effect toward various microrganisms.[10,57,58] Compared with Ag-$CoFe_2O_4$, Ag-$CoFe_2O_4$-GO exhibits a higher antibacterial ability at the same concentration toward both bacteria. Similarly, $CoFe_2O_4$-GO always showed a better bactericidal effect than $CoFe_2O_4$. GO and reduced graphene oxide (rGO) had been reported with excellent antibacterial activity toward *E. coli*.[59,60] Ag-$CoFe_2O_4$-GO nanocomposite in this work possessed a superlative antibacterial effect compared with $CoFe_2O_4$, Ag-$CoFe_2O_4$, and $CoFe_2O_4$-GO, suggesting that this improved antibacterial effect of Ag-$CoFe_2O_4$-GO was possibly attributed to the coordination of GO nanosheets and nano-Ag.[10,61] In Figure 4D, *S. aureus* exhibited negative values in viability treated with 6.25 and 12.5 μg/mL of $CoFe_2O_4$. It illustrated that $CoFe_2O_4$ had no inactivation effect toward *S. aureus* at low concentrations below 12.5 μg/mL. Tang et al. reported that graphene oxide-silver nanocomposite exhibited about 80% of antibacterial efficiency at a concentration of 10 μg/mL.[7] Tian et al. prepared GO-IONP-Ag as a novel multifunctional antibacterial material with 94.9% of *E. coli* inactivation at the final concentration of 8 μg/mL (silver content).[48] Deng et al. reported the synthesis of magnetic-graphene oxide which displayed 91.49% of inactivation at the concentration of 100 μg/mL.[49] Liu et al. reported that the loss of *E. coli* viability at the GO concentration of 80 μg/mL was 91.6%.[60] However, Ag-$CoFe_2O_4$-GO in this work exhibited the best antibacterial activity (compared to those mentioned above) with an *E. coli* inactivation of 98.8% even at a concentration as low as 6.25 μg/mL.

This significantly enhanced antibacterial efficiency for Ag-$CoFe_2O_4$-GO was supposed to be the result of the synergistical action between $CoFe_2O_4$-GO nanosheets and Ag nanoparticles. Therefore, the nano-Ag, $CoFe_2O_4$-GO, and the simple mixture of nano-Ag and $CoFe_2O_4$-GO at the same nano-Ag and $CoFe_2O_4$ concentrations were taken as controls, respectively. According to the EDS energy spectrum analysis of Ag-$CoFe_2O_4$-GO, the amount of Ag content is about 6.42%. As shown in Figure S8, Supporting Information, nano-Ag and the mixture of the two constituents also showed an antibacterial effect toward *E. coli* and *S. aureus* in a dose-dependent manner. At a Ag-$CoFe_2O_4$-GO concentration of 25 μg/mL (Ag concentration of 1.6 μg/mL and $CoFe_2O_4$-GO concentration of 23.4 μg/mL), the antibacterial rates of nano-Ag, $CoFe_2O_4$-GO, the simple mixture of these two constituents, and Ag-$CoFe_2O_4$-GO were 8.1%, 54.8%, 56.8%, and 99.8% toward *E. coli*, respectively. For *S. aureus*, these rates were 11.0%, 40.7%, 41.2%, and 99.4%, respectively. It indicated that Ag-$CoFe_2O_4$-GO nanocomposite exhibited better antibacterial efficiency than the simple sum of the $CoFe_2O_4$-GO and nano-Ag. Therefore, the enhanced antibacterial efficiency for Ag-$CoFe_2O_4$-GO could be attributed to the synergistical action of $CoFe_2O_4$-GO nanosheets and Ag nanoparticles instead of the simple mixture of the two constituents.

In addition, the Ag^+ and Co^{2+} concentrations had been measured using ICP (IRIS Intrepid II XSP, Thermo Elemental) to investigate the stability of Ag-$CoFe_2O_4$-GO. The Ag^+ and Co^{2+} release rate of the four different materials after 2 h of the antibacterial experiment toward *E. coli* (10^5 CFU/mL) was shown in Figure S9, Supporting Information. Compared with $CoFe_2O_4$ and Ag-$CoFe_2O_4$, their GO composites exhibited slower Ag^+ and Co^{2+} release rates, especially for Co^{2+} which decreased by more than three times, indicating the enhanced stability of Ag-$CoFe_2O_4$ nanoparticles after loading them on GO nanosheets. The results were consistent with the early report by Cao et al., who had found the slower Ag^+ release rate

DOI: 10.1021/acsami.5b02209
ACS Appl. Mater. Interfaces 2015, 7, 10576−10586

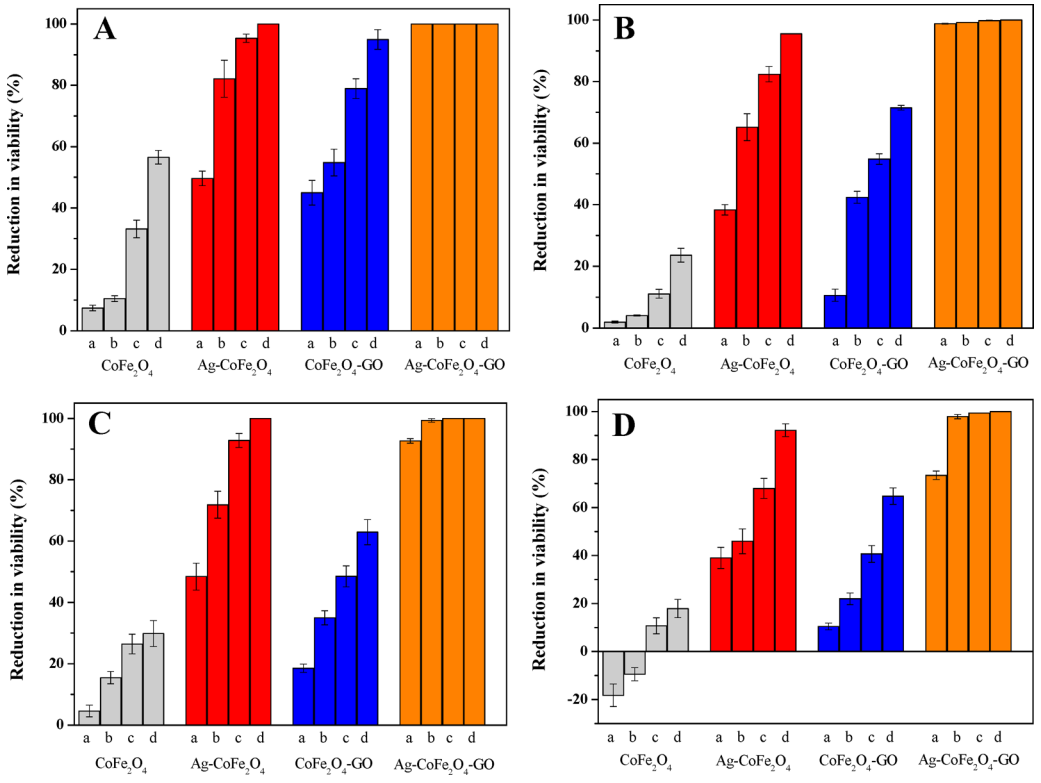

Figure 4. Reduction in viability of *E. coli* at 10^3 CFU/mL (A) and 10^5 CFU/mL (B) and of *S. aureus* at 10^3 CFU/mL (C) and 10^5 CFU/mL (D) after treatment with $CoFe_2O_4$, Ag-$CoFe_2O_4$, $CoFe_2O_4$-GO, and Ag-$CoFe_2O_4$-GO at different concentrations. a, b, c, and d represent the final concentrations of different materials at 6.25, 12.5, 25, and 50 μg/mL, respectively.

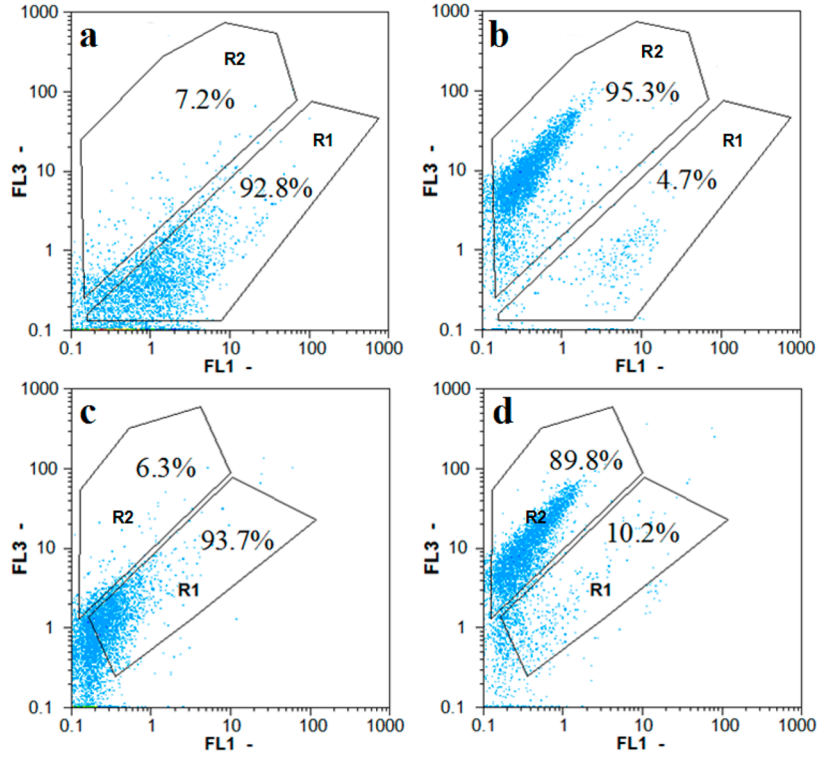

Figure 5. Flow cytometer dot plot of *E. coli* (a, b) and *S. aureus* (c, d) without (a, c) and with (b, d) Ag-$CoFe_2O_4$-GO treatment at 50 μg/mL for 2 h.

and better antibacterial activity of Ag@Fe_2O_3-GO nanocomposites than plain Ag and Ag@Fe_2O_3 nanomaterials.[61]

Fluorescent-Based Cell Live/Dead Test. The standard CFU counting method reflected the bacterial strains, which could not proliferate and divide. However, in fact, during the disinfection process, it was quite possible that there were many bacteria that were just reversibly injured by biocides, thus losing the ability to divide but being able to resuscitate after self-

DOI: 10.1021/acsami.5b02209
ACS Appl. Mater. Interfaces 2015, 7, 10576−10586

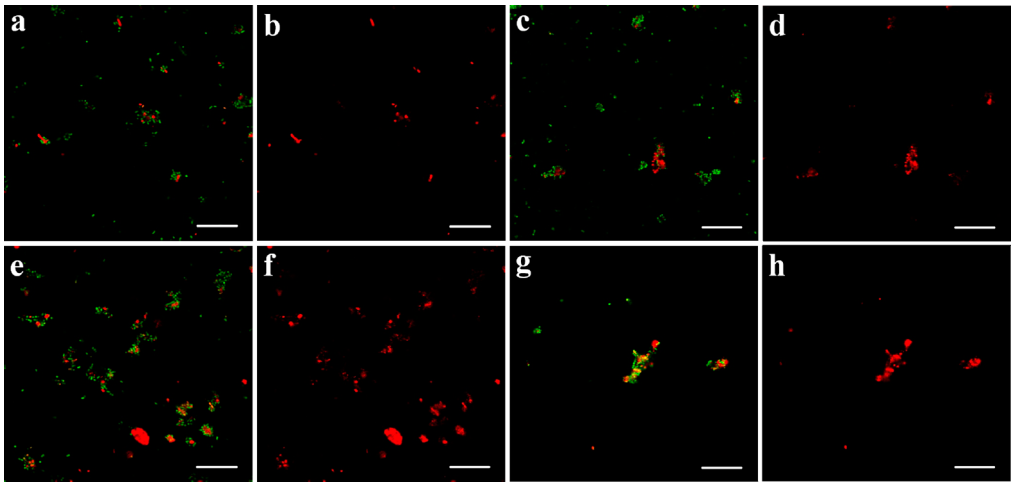

Figure 6. Confocal fluorescent images of live and dead bacterial cells treated with 50 μg/mL of Ag-$CoFe_2O_4$ (a–d) and Ag-$CoFe_2O_4$-GO (e–f) and stained with SYTO9 (green) and PI (red). (a, e) Overlying images of *E. coli* stained with SYTO9 (live and dead) and PI (dead). (b, f) Images of *E. coli* stained with PI. (c, g) Overlying images of *S. aureus* stained with SYTO9 (live and dead) and PI (dead). (d, h) Images of *S. aureus* stained with PI. The scale bar is 20 μm.

repair.[62] In order to verify whether the cells were harmed in a reversible manner or not, both bacterial species were examined using flow cytometer analysis. As shown in Figure 5a–d, the pictures exhibited the particular fluorescence pattern of *E. coli* (Figure 5a,b) and *S. aureus* (Figure 5c,d) doubly stained with SYTO9 and PI. The low red and strong green fluorescence intensity region (R1) represented the proportion of live bacteria, and the weak green and heavy red fluorescence intensity region (R2) indicated the dead proportion. For *E. coli*, 7.2% of cells without the addition of the nanomaterial fell in the R1, whereas the R1 values were 62.6%, 61.3%, and 95.3% for bacteria treated with 50 μg/mL of Ag-$CoFe_2O_4$, $CoFe_2O_4$-GO, and Ag-$CoFe_2O_4$-GO, respectively (Figures 5a, b and S10a–c, Supporting Information). In the case of *S. aureus*, the control presented 6.3% of dead bacteria, and Ag-$CoFe_2O_4$, $CoFe_2O_4$-GO and Ag-$CoFe_2O_4$-GO exhibited 43.4%, 34.4%, and 89.8% of disinfection (Figures 5c,d and S10d–f, Supporting Information). In the case of Ag-$CoFe_2O_4$, the antibacterial amounts determined by flow cytometry (62.6% and 43.4% against *E. coli* and *S. aureus*, respectively) were lower than those from the standard counting method (95.5% and 92.2% against *E. coli* and *S. aureus*, respectively). It was the same situation for $CoFe_2O_4$-GO (Figures 4 and S10c,f, Supporting Information). However, the differences of Ag-$CoFe_2O_4$-GO were not obvious as shown in Figures 4b,d and 5b,d. Therefore, Ag-$CoFe_2O_4$-GO inactivated both bacteria in a stronger manner than Ag-$CoFe_2O_4$ and $CoFe_2O_4$-GO. The confocal fluorescent images (Figure 6a–h) also demonstrated better antibacterial activities of Ag-$CoFe_2O_4$-GO than that of Ag-$CoFe_2O_4$. After treatments with Ag-$CoFe_2O_4$ and $CoFe_2O_4$-GO, a significant proportion of bacteria was just reversibly injured, losing the ability to divide but able to resuscitate after self-repair.[62] Therefore, the applications of $CoFe_2O_4$-GO and Ag-$CoFe_2O_4$ in microbial contaminated water treatment were inadvisible and unsafe.

Antibacterial Effects of Ag-$CoFe_2O_4$-GO with Different Process Factors. A series of experiments were conducted to investigate the influence of environmental factors such as temperature, time interval, and pH. On the basis of our results, it could be found that temperature was a significant factor influencing the activity of bacteria. In this work, both *E. coli* and *S. aureus* were very sensitive to inactivation temperature. As shown in Figure S11a, Supporting Information, the antibacterial rates were 75.4%, 80.5%, and 99.9% for *E. coli* at 25, 30, and 37 °C, respectively. However, the loss of *S. aureus* viability reached 61.3%, 70.7, and 99.9% after incubation for 2 h at 25, 30, and 37 °C, respectively. Although the antibacterial effect of Ag-$CoFe_2O_4$-GO was considerably influenced by the temperature, it possessed more than 60% of inactivation for both bacteria at 25 °C. To assess the effect of treatment time on antibacterial effect, the mixed suspension (PBS 0.01 mM, pH 7.0) of *E. coli* (or *S. aureus*) and Ag-$CoFe_2O_4$-GO with a concentration of 50 μg/mL was incubated on a rotary shaker at 180 rpm for different times (7.5, 15, 30, 60, 120 min). As shown in Figure S11b, Supporting Information, it was observed that the antibacterial effects increased gradually with the extension of incubation time and the inactivation amounts reached more than 90% after 60 min for both bacteria. The inactivation rate reached 94.5% and 50.6% against *E. coli* and *S. aureus* in 30 min, respectively. Obviously, the inactivation efficiency improved much faster for *E. coli* than *S. aureus* from 0 to 30 min. However, *E. coli* presented more susceptibility toward Ag-$CoFe_2O_4$-GO than *S. aureus* from 30 to 60 min. It was quite possible that the different cell wall/membrane structures of *E. coli* than *S. aureus* resulted in their different response to the incubation time. Wastewater fouled with bacteria could be variant in pH, and so, the influence of pH was evaluated during the inactivation process. As demonstrated in Figure S11c, Supporting Information, the antibacterial effect of Ag-$CoFe_2O_4$-GO (50 μg/mL) was more than 95% for both bacteria (10^5 CFU/mL) at different pH values (4, 5, 6, 7.2, 8, 9) after incubation for 2 h at 37 °C. The high adaptability of Ag-$CoFe_2O_4$-GO to different pH values justified its potential application in purifying actual wastewater with microbial contamination.

Different Antibacterial Effects toward *E. coli* and *S. aureus*. From Figure 4, it was easily found that all the nanocomposites presented higher antibacterial effects against *E. coli* than *S. aureus*. In the case of *S. aureus* (10^5 CFU/mL), after treatment with 12.5 μg/mL of $CoFe_2O_4$, Ag-$CoFe_2O_4$, $CoFe_2O_4$-GO, and Ag-$CoFe_2O_4$-GO, the loss of viability was 5.4%, 46.0%, 22.0%, and 97.9%, respectively. However, for *E. coli* at the same treatment, the inactivation amounts were 7.1%,

DOI: 10.1021/acsami.5b02209
ACS Appl. Mater. Interfaces 2015, 7, 10576–10586

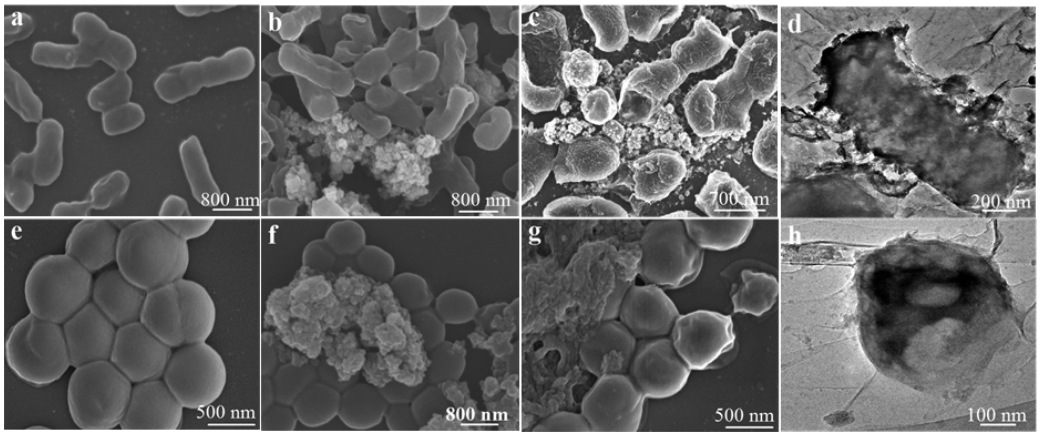

Figure 7. SEM images of *E. coli* (a, b, c) and *S. aureus* (e, f, g) without (a, e) and with Ag-$CoFe_2O_4$ (b, f) and Ag-$CoFe_2O_4$-GO (c, g) treatment at 50 μg/mL for 2 h. TEM images of *E. coli* (d) and *S. aureus* (h) with treatment of Ag-$CoFe_2O_4$-GO at the same conditions.

65.2%, 42.4%, and 99.2%, respectively. At the same time, *E. coli* (G−) and *S. aureus* (G+) exhibited different responses to the environmental factors such as incubation time and temperature. In brief, the *E. coli* was more easily inactivated by Ag-$CoFe_2O_4$-GO than *S. aureus*. To further investigate the underlying mechanism and inspect the bacterial morphological change, both bacterial strains were visualized using SEM and TEM technology. It was obvious that some of the bacterial strains were fixed on the GO plane and fused into the material (Figure 7c,d,g). Indeed, about 90% of *E. coli* with the addition of Ag-$CoFe_2O_4$-GO presented extensive damaged cell walls and cell membranes compared with the control (Figure 7a,e) and Ag-$CoFe_2O_4$ (Figure 7b,f) treatment. Remarkably, some of the cells were even drilled by Ag-$CoFe_2O_4$-GO forming big cavities on the cell surfaces which could cause the leakage of internal cell contents (Figure 7c). For the *S. aureus*, there were no signals of cellular division when treated with Ag-$CoFe_2O_4$-GO (Figure 7g). However, commenced cell division could be observed in control cells as showed in Figure 7e. Moreover, the cells absorbed on the Ag-$CoFe_2O_4$-GO shrank from a regular sphere to irregular shape forming pits on their surface (Figure 7g,h). It was interesting to note that some of the *S. aureus* cells incubated with Ag-$CoFe_2O_4$-GO (Figure 7g) seem to exhibit a plasmolysis phenomenon as compared with the control (Figure 7e) and Ag-$CoFe_2O_4$ (Figure 7f) treatment. It was quite possible that the double pressures from GO and nano-Ag were responsible for this morphological change of *S. aureus*. However, in the case of *S. aureus*, it was difficult to decide whether the integrity of the membrane was compromised from the SEM images. From the flow cytometer dot plot in Figure 5b,d, it was clear that Ag-$CoFe_2O_4$-GO possesses 95.3% and 89.8% inactivation of *E. coli* and *S. aureus*, respectively. Therefore, in light of the SEM results and together with the flow cytometer analysis, more than 95% of *E. coli* and around 90% of *S. aureus* presented severe membrane injury due to the addition of Ag-$CoFe_2O_4$-GO. According to the early reports, antibacterial activities were usually considered to be relative to the interaction between deterrents and cell membrane of bacteria.[10,63] It was well-known that the Gram-positive *S. aureus* had a multilayer (20−80 nm) positively charged dense peptidoglycan on its surface; however, Gram-negative *E. coli* possessed only one thin layer of lipopolysaccharide and peptidoglycan (15−20 nm) in its cell walls.[7,48] This structural difference was supposedly responsible for the antibacterial discrepancy. Furthermore, *S. aureus* contained more potent detoxification agents such as golden carotenoid pigments and catalase to resist oxidative stress,[63−65] which granted this bacteria more resistance and insusceptibility than *E. coli* under the same damaging treatment.

Simultaneous Disinfecting and Pb(II) Adsorbing Experiments. As shown in Figure S12a, Supporting Information, both *E. coli* and *S. aureus* (10^5 CFU/mL) exhibited negligible adsorption to Pb(II) with different concentrations of 1, 2, 4, 6, and 8 mg/L, respectively. On the other hand, 1, 2, 4, and 6 mg/L of Pb(II) have very little influence on the viability of both strains, except that the level of 8 mg/L shows around 20% and 32% of inhibition of *E. coli* and *S. aureus*, respectively (Figure S12b, Supporting Information). For the individual Pb(II) adsorption experiment, the $CoFe_2O_4$-GO exhibited the best removal efficiency (Figure 8a,b). The adsorption q_e for Pb(II) with an initial concentration of 6 mg/L using $CoFe_2O_4$, Ag-$CoFe_2O_4$, $CoFe_2O_4$-GO, and Ag-$CoFe_2O_4$-GO was 50.2, 42.9, 81.3, and 60.8 mg/g, respectively. The Pb(II) adsorption data had been analyzed according to the Langmuir (Figure 8a) and Freundlich (Figure S13, Supporting Information) model.[66] As shown in Table S1, Supporting Information, the Langmuir model showed a correlation coefficient of 0.927, 0.963, 0.925, and 0.996 for $CoFe_2O_4$, Ag-$CoFe_2O_4$, $CoFe_2O_4$-GO, and Ag-$CoFe_2O_4$-GO, respectively. Our results indicated that the Freundlich model fitted the data with a correlation coefficient of 0.775, 0.874, 0.910, and 0.877, respectively. Therefore, the Langmuir model could provide a better representation of the adsorption isotherms of Pb(II) than the Freundlich model, which was consistent with the earlier report by Madadrang et al.[67] The removal amount of Pb(II) (6 mg/L) was 58.0%, 47.0%, 81.5%, and 70.1% by Ag-$CoFe_2O_4$, $CoFe_2O_4$-GO, $CoFe_2O_4$-GO, and Ag-$CoFe_2O_4$-GO, respectively. The surface area of $CoFe_2O_4$, Ag-$CoFe_2O_4$, $CoFe_2O_4$-GO, and Ag-$CoFe_2O_4$-GO was 100.4, 89.2, 212.7, and 140.8 m^2/g, respectively. It was obvious that Pb(II) removal efficiency in this work had a significant dependence on the surface area and isoelectric point (Figure S12c, Supporting Information). Ag-$CoFe_2O_4$-GO showed relatively lower Pb(II) removal efficiency than $CoFe_2O_4$-GO. It seemed that more adsorption sites were taken up by nano-Ag besides $CoFe_2O_4$ for Ag-$CoFe_2O_4$-GO. The high surface area and low isoelectric point (IEP) of $CoFe_2O_4$-GO and Ag-$CoFe_2O_4$-GO should be responsible for their better Pb(II) elimination compared with $CoFe_2O_4$ and Ag-$CoFe_2O_4$.[67,68] The results of simultaneous disinfection and Pb(II) adsorption experiments are given in

DOI: 10.1021/acsami.5b02209
ACS Appl. Mater. Interfaces 2015, 7, 10576−10586

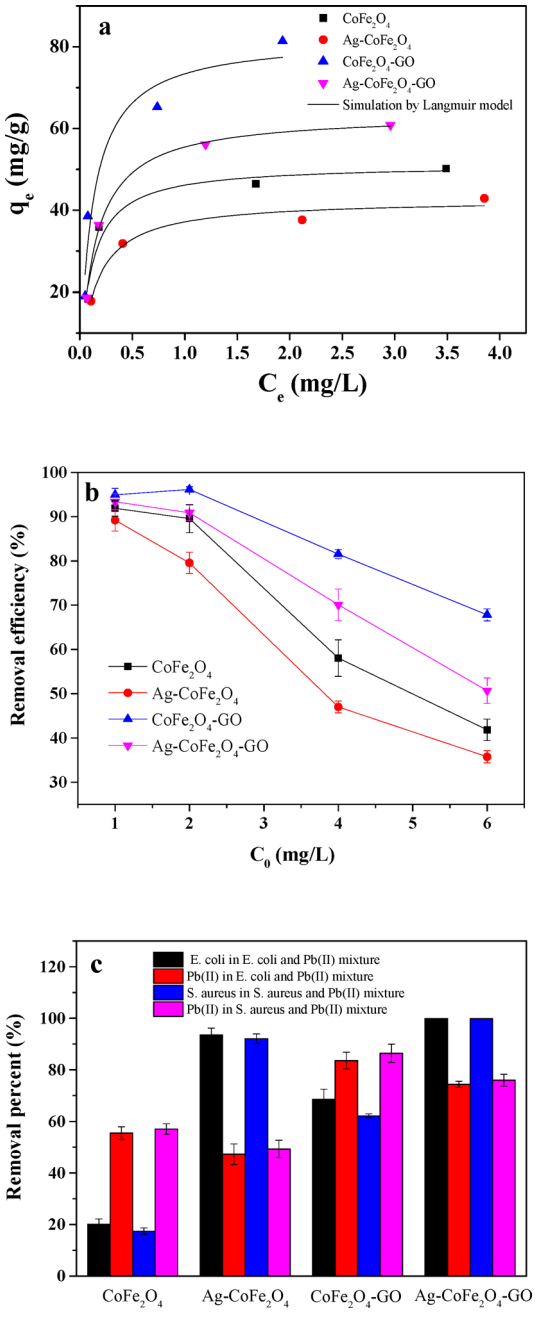

Figure 8. (a) Adsorption isotherms of Pb(II) simulated by the Langmuir model (temperature of 37 °C, pH 7, 2 h) with 50 μg/mL of $CoFe_2O_4$, Ag-$CoFe_2O_4$, $CoFe_2O_4$-GO, and Ag-$CoFe_2O_4$-GO, respectively. (b) Removal efficiency of Pb(II) at the same conditions as (a). (c) Removal percent of *E. coli* and Pb(II), *S. aureus* and Pb(II) in the mixtures of *E. coli* (10^5 CFU/mL) and Pb(II) (4 mg/L), and *S. aureus* (10^5 CFU/mL) and Pb(II) (4 mg/L) at the same conditions as (a), respectively.

Figure 8c. For the *E. coli* and Pb(II) mixture, Ag-$CoFe_2O_4$, $CoFe_2O_4$-GO, $CoFe_2O_4$-GO, and Ag-$CoFe_2O_4$-GO possessed 20.2%, 93.5%, 68.5%, and 99.9% of antibacterial efficiency and 55.5%, 47.3%, 83.6%, and 74.4% of Pb(II) adsorption, respectively. In the case of *S. aureus* and the Pb(II) mixture, these values were 17.4%, 92.1%, 62.2%, and 99.9% for disinfection and 57.1%, 49.3%, 86.4%, and 76.0% for Pb(II) removal, respectively. Generally, Ag-$CoFe_2O_4$-GO presents simultaneously more than 99% of antibacterial efficiency and around 75% of Pb(II) removal efficiency.

Antibacterial and Pb(II) Adsorption Mechanism of Ag-$CoFe_2O_4$-GO. In order to maximize the antibacterial and Pb(II) removal efficiency of Ag-$CoFe_2O_4$-GO, a comprehensive and in-depth understanding mechanism was necessary (Figure 9). GO, a highly oxidative form of graphene achieved by

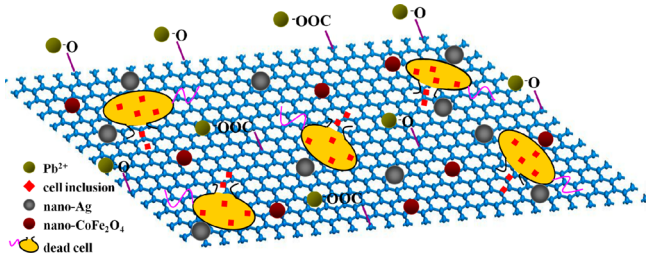

Figure 9. Antibacterial and Pb(II) adsorption mechanism of Ag-$CoFe_2O_4$-GO.

chemical exfoliation of graphite using $KMnO_4$ and H_2SO_4, possessed a giant specific surface area and contained a large amount of oxygenic functional groups such as carboxyl, hydroxyl, and epoxy, which made them form more stable and uniform dispersion and thus provided more opportunities for contact with bacteria and Pb(II) compared with nanomaterials without GO (Figures S14 and S15, Supporting Information). As shown in Figure 1a,b, $CoFe_2O_4$ and Ag-$CoFe_2O_4$ seriously aggregated compared with $CoFe_2O_4$-GO and Ag-$CoFe_2O_4$-GO. Moreover, the nano-Ag deposited on the GO plane exhibited narrower and smaller diameters (40−50 nm) than those (50−100 nm) without GO. It was generally accepted that the antibacterial activity of nanomaterials shows a significant size effect, that is, smaller particles presented stronger disinfection control.[63,69] The better dispersity of Ag-$CoFe_2O_4$-GO (Figure 1f) provided more opportunities for it to come into contact with bacteria and so had a contribution to the prominent disinfection activity of Ag-$CoFe_2O_4$-GO. The Ag-$CoFe_2O_4$-GO treated *E. coli* in this work were damaged seriously in their membrane with big cavities in their surface. Graphene related nanomaterials were capable of oxidizing bacterial proteins, lipids, and DNA.[60] On the other hand, the antibacterial activity of nano-Ag had been well accepted and applied since ancient times. Nano-Ag could adhere on the membrane of bacteria, degrade lipopolysaccharide molecules, cause large increases in membrane permeability, and then penetrate inside the bacterial cell, resulting in DNA damage and ultimately the death of bacteria.[70] In this work, we proposed a four-step approach to reveal an antibacterial and Pb(II) removal mechanism. First, the bacteria and Pb(II) were adsorbed and deposited on the plane of GO. GO had a significant and delocalized π-bonding system perpendicular to its plane. On the one hand, most nucleic acid, proteins, and other biomacromolecules had aromaticity.[43] The nonspecific binding of cells with GO induced by π-stacking interactions should be responsible for the absorption of bacteria on GO. On the other hand, the electrostatic interaction between the carboxyl and hydroxyl of GO and Pb(II) might explain its prominent Pb(II) absorption. Second, the GO plane curled like the nanotube and wrapped up the cells (Figure S16, Supporting Information). It was reported that graphene was not absolutely flat, and in fact, it presented intrinsic and nanometer-scale coarseness and corrugation.[71] Thus, the GO could envelop bacteria (Figure S16, Supporting Information),

DOI: 10.1021/acsami.5b02209
ACS Appl. Mater. Interfaces 2015, 7, 10576−10586

restrict their free activities, and cause physical pressure on the cell membrane.[43,72] Third, after cells were deposited and confined on the GO plane, nano-Ag came into contact with the cell membrane, which together with GO changed the permeability of the functional membrane by oxidizing the lipids and proteins in the membrane and resulted in pits and holes on the surface and the malfunction of selective permeable barriers.[73,74] Fourth, the internal contents of the cells were leaked, and the DNA was damaged because of the penetration of nano-Ag and release of Ag^+.[70,75,76] Eventually, the bacteria were killed in an irreversible manner. In a word, taking into consideration the easy magnetic separation of Ag-$CoFe_2O_4$-GO, it was the very promising candidate material for advanced antimicrobial and Pb(II) contaminated water treatment.

CONCLUSIONS

In this paper, Ag-$CoFe_2O_4$-graphene oxide (Ag-$CoFe_2O_4$-GO) nanocomposite was synthesized to purify both bacteria and Pb(II) contaminated water. The Ag-$CoFe_2O_4$-GO nanomaterial was characterized by TEM, XRD, FTIR, Raman, XPS, Brunauer-Emmett-Teller (BET), CV, and magnetic property tests. Ag-$CoFe_2O_4$-GO exhibited the simultaneous superior removal efficiency of bacteria and Pb(II) compared with $CoFe_2O_4$, Ag-$CoFe_2O_4$, and $CoFe_2O_4$-GO composite. The antibacterial mechanism was also discussed in detail to have a better understanding of the interaction between Ag-$CoFe_2O_4$-GO and bacteria. Generally, taking into account its easy magnetic separation, bulk availability, and irreversibly high antibacterial activity, Ag-$CoFe_2O_4$-GO was an ideal nanomaterial for complex microbial and Pb(II) contaminated water treatment.

ASSOCIATED CONTENT

Supporting Information

Additional data about chemicals, STEM-EDX line scanning, FTIR, XRD, Raman and XPS spectrum, N_2 adsorption and desorption isotherms, the synergistical action of nano-Ag and $CoFe_2O_4$-GO nanosheets, flow cytometer dot plot, the influences of temperature, time, and pH, the mutual influences between bacteria and Pb(II), adsorption isotherms of Pb(II) simulated by the Freundlich model, optical microscope images showing the interactions between bacteria and materials, and TEM picture showing GO-wrapping of bacteria. The Supporting Information is available free of charge on the ACS Publications website at DOI: 10.1021/acsami.5b02209.

AUTHOR INFORMATION

Corresponding Authors

*E-mail: sihuizhan@nankai.edu.cn. Phone: +86-022-23507800. Fax: +86-022-66229562.

*E-mail: zhouqx523@yahoo.com. Phone: +86-022-23507800. Fax: +86-022-66229562.

Notes

The authors declare no competing financial interest.

ACKNOWLEDGMENTS

The authors gratefully acknowledge the financial support provided by the National Natural Science Foundation of China as general projects (21377061 and 31170473) and a joint Guangdong project (U1133006) and the Key Technologies R&D Program of Tianjin (13ZCZDSF00300).

REFERENCES

(1) Philip, S. S.; Costerton, J. W.; Greenberg, E. P. Bacterial Biofilms: A Common Cause of Persistent Infections. *Science* **1999**, *284*, 1318−1322.

(2) Tong, T. Z.; Shereef, A.; Wu, J. S.; Binh, C. T. T.; Kelly, J. J.; Gaillard, J.; Gray, K. A. Effects of Materials Morphology on the Phototoxicity of Nano-TiO_2 to Bacteria. *Environ. Sci. Technol.* **2013**, *47*, 12486−12495.

(3) Adegboyega, N. F.; Sharma, V. K.; Siskova, K. M.; Vecerova, R.; Kolar, M.; Zboril, R.; Gardea-Torresdey, J. L. Enhanced Formation of Silver Nanoparticles in Ag^+-NOM-Iron(II, III) Systems and Antibacterial Activity Studies. *Environ. Sci. Technol.* **2014**, *48*, 3228−3235.

(4) Wang, W. J.; Yu, J. C.; Xia, D. H.; Wong, P. K.; Li, Y. C. Graphene and g-C_3N_4 Nanosheets Cowrapped Elemental α-Sulfur as a Novel Metal-Free Heterojunction Photocatalyst for Bacterial Inactivation under Visible-Light. *Environ. Sci. Technol.* **2013**, *47*, 8724−8732.

(5) Ben-Sasson, M.; Zodrow, K. R.; Qi, G.; Yan, K.; Giannelis, E. P.; Elimelech, M. Surface Functionalization of Thin-Film Composite Membranes with Copper Nanoparticles for Antimicrobial Surface Properties. *Environ. Sci. Technol.* **2014**, *48*, 384−393.

(6) Sassman, S. A.; Lee, L. S. Sorption of Three Tetracyclines by Several Soils: Assessing the Role of pH and Cation Exchange. *Environ. Sci. Technol.* **2005**, *39*, 7452−7459.

(7) Tang, J.; Chen, Q.; Xu, L. G.; Zhang, S.; Feng, L. Z.; Cheng, L.; Xu, H.; Liu, Z.; Peng, R. Graphene Oxide-Silver Nanocomposite as a Highly Effective Antibacterial Agent with Species-Specific Mechanisms. *ACS Appl. Mater. Interfaces* **2013**, *5*, 3867−3874.

(8) Shen, J. F.; Shi, M.; Li, N.; Yan, B.; Ma, H. W.; Hu, Y. Z.; Ye, M. X. Facile Synthesis and Application of Ag-Chemically Converted Graphene Nanocomposties. *Nano Res.* **2010**, *3*, 339−349.

(9) Zhu, Y. J.; Ramasamy, M.; Yi, D. K. Antibacterial Activity of Ordered Gold Nanorod Arrays. *ACS Appl. Mater. Interfaces* **2014**, *6*, 15078−15085.

(10) Martinez, J. L. Antibiotics and Antibiotic Resistance Genes in Natural Environments. *Science* **2008**, *321*, 365−367.

(11) Glover, R. D.; Miller, J. M.; Hutchison, J. E. Generation of Metal Nanoparticles from Silver and Copper Objects: Nanoparticle Dynamics on Surfaces and Potential Sources of Nanoparticles in the Environment. *ACS Nano* **2011**, *5*, 8950−8957.

(12) Christensen, F. M.; Johnston, H. J.; Stone, V. Nano-Silver-Feasibility and Challenges for Human Health Risk Assessment Based on Open Literature. *Nanotoxicology* **2010**, *4*, 284−295.

(13) Ansari, M. I.; Malik, A. Biosorption of Nickel and Cadmium by Metal Resistant Bacterial Isolates from Agricultural Soil Irrigated with Industrial Wastewater. *Bioresour. Technol.* **2007**, *98*, 3149−3153.

(14) Li, Y. H.; Di, Z. C.; Ding, J.; Wu, D. H.; Luan, Z. K.; Zhu, Y. Q. Adsorption Thermodynamic, Kinetic and Adsorption Studies of Pb^{2+} on Carbon Nanotubes. *Water Res.* **2005**, *39*, 605−609.

(15) Machida, M.; Mochimaru, T.; Tatsumoto, H. Lead(II) Adsorption onto the Graphene Layer of Carbonaceous Materials in Aqueous Solution. *Carbon* **2006**, *44*, 2681−2688.

(16) *Guidelines for Drinking Water Quality*; World Health Organization: Geneva, Switzerland, 1984; pp 1−2.

(17) Zhang, X.; Lin, S.; Chen, Z. L.; Megharaj, M.; Naidu, R. Kaolinite-Supported Nanoscale Zero-Valent Iron for Removal of Pb^{2+} from Aqueous Solution: Reactivity, Characterization and Mechanism. *Water Res.* **2011**, *45*, 3481−3488.

(18) Ludwig, R. D.; Smyth, D. J. A.; Blowes, D. W.; Spink, L. E.; Wilkin, R. T.; Jewett, D. G.; Weisener, C. J. Treatment of Arsenic, Heavy Metals, and Acidity Using a Mixed ZVI-Compost PRB. *Environ. Sci. Technol.* **2009**, *43*, 1970−1976.

(19) Liu, J. F.; Zhao, Z. S.; Jiang, G. B. Coating Fe_3O_4 Magnetic Nanoparticles with Humic Acid for High Efficient Removal of Heavy Metals in Water. *Environ. Sci. Technol.* **2008**, *42*, 6949−6954.

(20) Zhan, S. H.; Yang, Y.; Shen, Z. Q.; Shan, J. J.; Li, Y.; Yang, S. S.; Zhu, D. D. Efficient Removal of Pathogenic Bacteria and Viruses by

DOI: 10.1021/acsami.5b02209
ACS Appl. Mater. Interfaces 2015, 7, 10576−10586

Multifunctional Amine-Modified Magnetic Nanoparticles. *J. Hazard. Mater.* **2014**, *274*, 115−123.
(21) Yantasee, W.; Warner, C. L.; Sangvanich, T.; Addleman, R. S.; Carter, T. G.; Wiacek, R. J.; Fryxell, G. E.; Timchalk, C.; Warner, M. G. Removal of Heavy Metals from Aqueous Systems with Thiol Functionalized Superparamagnetic Nanoparticles. *Environ. Sci. Technol.* **2007**, *41*, 5114−5119.
(22) Gupta, V. K.; Agarwal, S.; Saleh, T. A. Synthesis and Characterization of Alumina-Coated Carbon Nanotubes and Their Application for Lead Removal. *J. Hazard. Mater.* **2011**, *185*, 17−23.
(23) Saleh, T. A.; Gupta, V. K. Column with CNT/Magnesium Oxide Composite for Lead(II) Removal from Water. *Environ. Sci. Pollut. Res.* **2012**, *19*, 1224−1228.
(24) Lee, C.; Wei, X. D.; Kysar, J. W.; Hone, J. Measurement of the Elastic Properties and Intrinsic Strength of Monolayer Graphene. *Science* **2008**, *321*, 385−388.
(25) Nair, R. R.; Blake, P.; Grigorenko, A. N.; Novoselov, K. S.; Booth, T. J.; Stauber, T.; Peres, N. M. R.; Geim, A. K. Fine Structure Constant Defines Visual Transparency of Graphene. *Science* **2008**, *320*, 1308−1308.
(26) Xia, H.; Hong, C. Y.; Li, B.; Zhao, B.; Lin, Z. X.; Zheng, M. B.; Savilov, S. V.; Aldoshin, S. M. Facile Synthesis of Hematite Quantum-Dot/Functionalized Graphene-Sheet Composites as Advanced Anode Materials for Asymmetric Supercapacitors. *Adv. Funct. Mater.* **2015**, *25*, 627−635.
(27) Xia, H.; Zhu, D. D.; Fu, Y. S.; Wang, X. $CoFe_2O_4$-Graphene Nanocomposites as a High-Capacity Anode Material for Lithium-Ion Batteries. *Electrochim. Acta* **2012**, *83*, 166−174.
(28) Balandin, A. A.; Ghosh, S.; Bao, W.; Calizo, I.; Teweldebrhan, D.; Miao, F.; Lau, C. N. Superior Thermal Conductivity of Single-Layer Graphene. *Nano Lett.* **2008**, *8*, 902−907.
(29) Stankovich, S.; Dikin, D. A.; Dommett, G. H. B.; Kohlhaas, K. M.; Zimney, E. J.; Stach, E. A.; Piner, R. D.; Nguyen, S. T.; Ruoff, R. S. Graphene-Based Composite Materials. *Nature* **2006**, *442*, 282−286.
(30) Novoselov, K. S.; Geim, A. K.; Morozov, S. V.; Jiang, D.; Zhang, Y.; Dubonos, S. V.; Grigorieva, I. V.; Firsov, A. A. Electric Field Effect in Atomically Thin Carbon Films. *Science* **2004**, *306*, 666−669.
(31) Hummers, W. S.; Offeman, R. E. Preparation of Graphitic Oxide. *J. Am. Chem. Soc.* **1958**, *80*, 1339−1339.
(32) Park, S. J.; Ruoff, R. S. Chemical Methods for the Production of Graphenes. *Nat. Nanotechnol.* **2009**, *4*, 217−224.
(33) Liu, T. H.; Li, Y. H.; Du, Q. D.; Sun, J. K.; Jiao, Y. Q.; Yang, G. M.; Wang, Z. H.; Xia, Y. Z.; Zhang, W.; Wang, K. L.; Zhu, H. W.; Wu, D. H. Adsorption of Methylene Blue from Aqueous Solution by Graphene. *Colloids Surf., B* **2012**, *90*, 197−203.
(34) Ramesha, G. K.; Kumara, A. V.; Muralidhara, H. B.; Sampath, S. J. Graphene and Graphene Oxide as Effective Adsorbents toward Anionic and Cationic Dyes. *J. Colloid Interface Sci.* **2011**, *361*, 270−277.
(35) Huang, Z. H.; Zheng, X. Y.; Lv, W.; Wang, M.; Yang, Q. H.; Kang, F. Y. Adsorption of Lead (II) Ions from Aqueous Solution on Low-Temperature Exfoliated Graphene Nanosheets. *Langmuir* **2011**, *27*, 7558−7562.
(36) Sitko, R.; Turek, E.; Zawisza, B.; Malicka, E.; Talik, E.; Heinman, J.; Gagor, A.; Feist, B.; Wrzalik, R. Adsorption of Divalent Metal Ions from Aqueous Solutions Using Graphene Oxide. *Dalton Trans.* **2013**, *42*, 5682−5689.
(37) Beless, B.; Rifai, H. S.; Rodrigues, D. F. Efficacy of Carbonaceous Materials for Sorbing Polychlorinated Biphenyls from Aqueous Solution. *Environ. Sci. Technol.* **2014**, *48*, 10372−10379.
(38) Wu, T.; Cai, X.; Tan, S. Z.; Li, H. Y.; Liu, J. S.; Yang, W. D. Adsorption Characteristics of Acrylonitrile, *p*-Toluenesulfonic Acid, 1-Naphthalenesulfonic Acid and Methyl Blue on Graphene in Aqueous Solutions. *Chem. Eng. J.* **2011**, *173*, 144−149.
(39) Lyon, D. Y.; Adams, L. K.; Falkner, J. C.; Alvarez, P. J. J. Antibacterial Activity of Fullerene Water Suspensions: Effects of Preparation Method and Particle Size. *Environ. Sci. Technol.* **2006**, *40*, 4360−4366.
(40) Mauter, M. S.; Elimelech, M. Environmental Applications of Carbon-Based Nanomaterials. *Environ. Sci. Technol.* **2008**, *42*, 5843−5859.
(41) Hu, W. B.; Peng, C.; Luo, W. J.; Lv, M.; Li, X. M.; Li, D.; Huang, Q.; Fan, C. H. Graphene-Based Antibacterial Paper. *ACS Nano* **2010**, *4*, 4317−4323.
(42) Akhavan, O.; Ghaderi, E. Toxicity of Graphene and Graphene Oxide Nanowalls against Bacteria. *ACS Nano* **2010**, *4*, 5731−5736.
(43) Hu, X. G.; Zhou, Q. X. Health and Ecosystem Risks of Graphene. *Chem. Rev.* **2013**, *113*, 3815−3835.
(44) Hu, X. G.; Mu, L.; Kang, J.; Lu, K. C.; Zhou, R. R.; Zhou, Q. X. Humic Acid Acts as a Natural Antidote of Graphene by Regulating Nanomaterial Translocation and Metabolic Fluxes in Vivo. *Environ. Sci. Technol.* **2014**, *48*, 6919−6927.
(45) Vadahanambi, S.; Lee, S. H.; Kim, W. J.; Oh, I. K. Arsenic Removal from Contaminated Water Using Three-Dimensional Graphene-Carbon Nanotube-Iron Oxide Nanostructures. *Environ. Sci. Technol.* **2013**, *47*, 10510−10517.
(46) Chandra, V.; Park, J.; Chun, Y.; Lee, J. W.; Hwang, I.; Kim, K. S. Water-Dispersible Magnetite-Reduced Graphene Oxide Composites for Arsenic Removal. *ACS Nano* **2010**, *4*, 3979−3986.
(47) Wu, X. L.; Wang, L.; Chen, C. L.; Xu, A. W.; Wang, X. K. Water-Dispersible Magnetite-Graphene-LDH Composites for Efficient Arsenate Removal. *J. Mater. Chem.* **2011**, *21*, 17353−17359.
(48) Tian, T. F.; Shi, X. Z.; Cheng, L.; Luo, Y. C.; Dong, Z. L.; Gong, H.; Xu, L. G.; Zhong, Z. T.; Peng, R.; Liu, Z. Graphene-Based Nanocomposite as an Effective, Multifunctional, and Recyclable Antibacterial Agent. *ACS Appl. Mater. Interfaces* **2014**, *6*, 8542−8548.
(49) Deng, C. H.; Gong, J. L.; Zeng, G. M.; Niu, C. G.; Niu, Q. Y.; Zhang, W.; Liu, H. Y. Inactivation Performance and Mechanism of *Escherichia coli* in Aqueous System Exposed to Iron Oxide Loaded Graphene Nanocomposites. *J. Hazard. Mater.* **2014**, *276*, 66−76.
(50) Markova, Z.; Siskova, K. M.; Filip, J.; Cuda, J.; Kolar, M.; Safarova, K.; Medrik, I.; Zboril, R. Air Stable Magnetic Bimetallic Fe-Ag Nanocomposites for Advanced Antimicrobial Treatment and Phosphorus Removal. *Environ. Sci. Technol.* **2013**, *47*, 5285−5293.
(51) Li, J.; Zhang, S. W.; Chen, C. L.; Zhao, G. X.; Yang, X.; Li, J. X.; Wang, X. K. Removal of Cu(II) and Fulvic Acid by Graphene Oxide Nanosheets Decorated with Fe_3O_4 Nanoparticles. *ACS Appl. Mater. Interfaces* **2012**, *4*, 4991−5000.
(52) Yang, S. B.; Hu, J.; Chen, C. L.; Shao, D. D.; Wang, X. K. Mutual Effects of Pb(II) and Humic Acid Adsorption on Multiwalled Carbon Nanotubes/Polyacrylamide Composites from Aqueous Solutions. *Environ. Sci. Technol.* **2011**, *45*, 3621−3627.
(53) Tokuyama, H.; Hisaeda, J.; Nii, S.; Sakohara, S. Removal of Heavy Metal Ions and Humic Acid from Aqueous Solutions by Co-Adsorption onto Thermosensitive Polymers. *Sep. Purif. Technol.* **2010**, *71*, 83−88.
(54) Li, X. J.; Guo, Z. K.; Li, J. X.; Zhang, Y.; Ma, H. M.; Pang, X. H.; Du, B.; Wei, Q. Quenched Electrochemiluminescence of Ag Nanoparticles Functionalized g-C_3N_4 by Ferrocene for Highly Sensitive Immunosensing. *Anal. Chim. Acta* **2015**, *854*, 40−46.
(55) Zhang, Y. K.; Yan, T.; Yan, L. G.; Guo, X. Y.; Cui, L. M.; Wei, Q.; Du, B. Preparation of Novel Cobalt Ferrite/Chitosan Grafted with Graphene Composite as Effective Adsorbents for Mercury Ions. *J. Mol. Liq.* **2014**, *198*, 381−387.
(56) Xia, H.; Hong, C. Y.; Shi, X. Q.; Li, B.; Yuan, G. L.; Yao, Q. F.; Xie, J. P. Hierarchical Heterostructures of Ag Nanocomposites Decorated MnO_2 Nanowires as Promising Electrodes for Supercapacitors. *J. Mater. Chem. A* **2015**, *3*, 1216−1221.
(57) Li, C.; Wang, X. S.; Chen, F.; Zhang, C. L.; Zhi, X.; Wang, K.; Cui, D. X. The Antifungal Activity of Graphene Oxide-Silver Nanocomposites. *Biomaterials* **2013**, *34*, 3882−3890.
(58) Mei, S. L.; Wang, H. Y.; Wang, W.; Tong, L. P.; Pan, H. B.; Ruan, C. S.; Ma, Q. L.; Liu, M. Y.; Yang, H. L.; Zhang, L.; Cheng, Y. C.; Zhang, Y. M.; Zhao, L. Z.; Chu, P. K. Antibacterial Effects and Biocompatibility of Titanium Surfaces with Graded Silver Incorporation in Titania Nanotubes. *Biomaterials* **2014**, *35*, 4255−4265.

DOI: 10.1021/acsami.5b02209
ACS Appl. Mater. Interfaces 2015, 7, 10576−10586

(59) Tu, Y. S.; Lv, M.; Xiu, P.; Huynh, T.; Zhang, M.; Castelli, M.; Liu, Z. R.; Huang, Q.; Fan, C. H.; Fang, H. P.; Zhou, R. H. Destructive Extraction of Phospholipids from *Escherichia coli* Membranes by Graphene Nanosheets. *Nat. Nanotechnol.* **2013**, *8*, 594−601.
(60) Liu, S. B.; Zeng, T. H.; Hofmann, M.; Burcombe, E.; Wei, J.; Jiang, R.; Kong, J.; Chen, Y. Antibacterial Activity of Graphite, Graphite Oxide, Graphene Oxide, and Reduced Graphene Oxide: Membrane and Oxidative Stress. *ACS Nano* **2011**, *5*, 6971−6980.
(61) Cao, N.; Chen, Y. J.; Jiang, J. Ag@Fe_2O_3-GO Nanocomposites Prepared by a Phase Transfer Method with Long-Term Antibacterial Property. *ACS Appl. Mater. Interfaces* **2013**, *5*, 11307−11314.
(62) Gelover, S.; Gomez, L. A.; Reyes, K.; Leal, M. T. A Practical Demonstration of Water Disinfection Using TiO_2 Films and Sunlight. *Water Res.* **2006**, *40*, 3274−3280.
(63) Applerot, G.; Lipovsky, A.; Dror, R.; Perkas, N.; Nitzan, Y.; Lubart, R.; Gedanken, A. Enhanced Antibacterial Activity of Nanocrystalline ZnO due to Increased ROS-Mediated Cell Injury. *Adv. Funct. Mater.* **2009**, *19*, 842−852.
(64) Liu, G. Y.; Essex, A.; Buchanan, J. T.; Datta, V.; Hoffman, H. M.; Bastian, J. F.; Fierer, J.; Nizet, V. *Staphylococcus aureus* Golden Pigment Impairs Neutrophil Killing and Promotes Virulence through Its Antioxidant Activity. *J. Exp. Med.* **2005**, *202*, 209−215.
(65) Schwartz, C. E.; Krall, J.; Norton, L.; McKay, K.; Kay, D.; Lynch, R. E. Catalase and Superoxide Dismutase in *Escherichia coli*. *J. Biol. Chem.* **1983**, *258*, 6277−6281.
(66) Qi, X. H.; Li, L. Y.; Tan, T. F.; Chen, W. T.; Smith, R. L. Adsorption of 1-Butyl-3-methylimidazolium Chloride Ionic Liquid by Functional Carbon Microspheres from Hydrothermal Carbonization of Cellulose. *Environ. Sci. Technol.* **2013**, *47*, 2792−2798.
(67) Madadrang, C. J.; Kim, H. Y.; Gao, G. H.; Wang, N.; Zhu, J.; Feng, H.; Gorring, M.; Kasner, M. L.; Hou, S. F. Adsorption Behavior of EDTA-Graphene Oxide for Pb(II) Removal. *ACS Appl. Mater. Interfaces* **2012**, *4*, 1186−1193.
(68) Kumar, S.; Nair, R. R.; Pillai, P. B.; Gupta, S. N.; Lyengar, M. A. R.; Sood, A. K. Graphene Oxide-$MnFe_2O_4$ Magnetic Nanohybrids for Efficient Removal of Lead and Arsenic from Water. *ACS Appl. Mater. Interfaces* **2014**, *6*, 17426−17436.
(69) Gogoi, S. K.; Gopinath, P.; Paul, A.; Ramesh, A.; Ghosh, S. S.; Chattopadhyay, A. Green Fluorescent Protein-Expressing *Escherichia coli* as a Model System for Investigating the Antimicrobial Activities of Silver Nanoparticles. *Langmuir* **2006**, *22*, 9322−9328.
(70) Li, Q. L.; Mahendra, S.; Lyon, D. Y.; Brunet, L.; Liga, M. V.; Li, D.; Alvarez, P. J. J. Antimicrobial Nanomaterials for Water Disinfection and Microbial Control: Potential Applications and Implications. *Water Res.* **2008**, *42*, 4591−4602.
(71) Meyer, J. C.; Geim, A. K.; Katsnelson, M. I.; Novoselov, K. S.; Booth, T. J.; Roth, S. The Structure of Suspended Graphene Sheets. *Nature* **2007**, *446*, 60−63.
(72) Mohanty, N.; Fahrenholtz, M.; Nagaraja, A.; Boyle, D.; Berry, V. Impermeable Graphenic Encasement of Bacteria. *Nano Lett.* **2011**, *11*, 1270−1275.
(73) Morones, J. R.; Elechiguerra, J. L.; Camacho, A.; Holt, K.; Kouri, J. B.; Ramirez, J. T.; Yacaman, M. J. The Bactericidal Effect of Silver Nanoparticles. *Nanotechnology* **2005**, *16*, 2346−2353.
(74) Rai, M. K.; Deshmukh, S. D.; Ingle, A. P.; Gade, A. K. Silver Nanoparticles: The Powerful Nanoweapon against Multidrug-Resistant Bacteria. *J. Appl. Microbiol.* **2012**, *112*, 841−852.
(75) Matsumura, Y.; Yoshikata, K.; Kunisaki, S.; Tsuchido, T. Mode of Bactericidal Action of Silver Zeolite and Its Comparison with That of Silver Nitrate. *Appl. Environ. Microbiol.* **2003**, *69*, 4278−4281.
(76) Feng, Q. L.; Wu, J.; Chen, G. Q.; Cui, F. Z.; Kim, T. N.; Kim, J. O. A Mechanistic Study of the Antibacterial Effect of Silver Ions on *Escherichia coli* and *Staphylococcus aureus*. *J. Biomed. Mater. Res.* **2000**, *52*, 662−668.

DOI: 10.1021/acsami.5b02209
ACS Appl. Mater. Interfaces 2015, 7, 10576−10586